

## Crystal chemistry of synthetic pyroxenes on the join $\text{CaNiSi}_2\text{O}_6$ - $\text{CaMgSi}_2\text{O}_6$ (diopside): A Rietveld structure refinement study

MATT RAUDSEPP, FRANK C. HAWTHORNE, ALLAN C. TURNOCK

Department of Geological Sciences, University of Manitoba, Winnipeg, Manitoba R3T 2N2, Canada

### ABSTRACT

A series of monoclinic  $C2/c$  pyroxenes was synthesized along the join  $\text{CaNiSi}_2\text{O}_6$ - $\text{CaMgSi}_2\text{O}_6$  (diopside). The crystal structures of these pyroxenes were refined with  $\text{CuK}\alpha$  X-ray powder data using the Rietveld method;  $R_b$  indices were in the range 2.7–3.7%. Cell parameters and mean bond lengths vary linearly as a function of composition along the join. However, the derived trends differ significantly from those of the  $\text{CaM}^{2+}\text{Si}_2\text{O}_6$  ( $\text{M}^{2+} = \text{Mg, Co, Fe, Mn}$ )  $C2/c$  pyroxenes. In particular, the slope of the  $\langle \text{M}(1)\text{-O} \rangle$  vs.  $\langle r_{\text{M}(1)} \rangle$  trend is 0.20, contrasting strongly with the slopes of the analogous relationship in the other calcic pyroxenes (slope = 0.89) and the hard-sphere model (slope = 1.0). Similar deviations occur at the large-cation end of the series  $\text{NaM}^{3+}\text{Si}_2\text{O}_6$  ( $\text{M}^{3+} = \text{Al, Cr, Fe, Sc, In}$ ) and  $\text{CaM}^{3+}\text{SiM}^{3+}\text{O}_6$  ( $\text{M}^{3+} = \text{Al, Fe, Sc}$ ). This type of anomalous behavior may be characteristic of anisodesmic structures close to their limits of chemical stability.

### INTRODUCTION

The crystal chemistry of the monoclinic pyroxenes has long been of interest. The structure will accept cations with a wide range of size and charge and is stable over a wide range of temperature and pressure. In the last 20 years, there has been a significant amount of work on end-member pyroxenes: synthesis, crystal structure refinement, spectroscopy, and the measurement of physical properties. Nevertheless, the behavior of minerals with this structure type continues to be intriguing. Of particular interest is the response of the structure to varying occupancy of the cation sites. This can be used in combination with site-occupancy refinement results to derive accurate site occupancies and is also of importance in fully understanding the crystal-chemical behavior of the pyroxene structure. General discussions of the latter topic are given by Clark et al. (1969), Ribbe and Prunier (1977), and Cameron and Papike (1981).

The monoclinic pyroxenes are conventionally divided into different series, depending on the occupancy of the  $\text{M}(2)$  cation site. Considering the Ca, Na, and Li pyroxenes together, there is approximate linearity of the metric stereochemical parameters (cell dimensions, mean bond lengths) with variation in the mean ionic radius of the constituent  $\text{M}(1)$  cation. However, close examination shows that there is significant nonlinearity in some of the relationships at very small or large constituent  $\text{M}(1)$ -cation radii. This is shown in the sodium pyroxenes by  $\text{NaInSi}_2\text{O}_6$  (Hawthorne and Grundy, 1974) and in the calcium pyroxenes by  $\text{CaNiSi}_2\text{O}_6$  (Ribbe and Prunier, 1977; Ghose et al., 1987). Here we further investigate the stereochemical behavior of the calcium pyroxene structure at small constituent cation radius by synthesis and characterization of solid solutions along the join  $\text{CaNi}$ -

$\text{Si}_2\text{O}_6$ - $\text{CaMgSi}_2\text{O}_6$  (diopside). As the synthesized material is very fine grained, Rietveld structure refinement was used to structurally characterize the resulting pyroxenes. Details of the method are reviewed by Young (1980) and Post and Bish (1989); application of the method to the characterization of pyroxenes along the diopside-hedenbergite join is described by Raudsepp et al. (1990).

### EXPERIMENTAL METHODS

#### Synthesis

Clinopyroxenes were synthesized from mixtures of dry reagent-grade  $\text{CaCO}_3$ ,  $\text{NiO}$ ,  $\text{SiO}_2$ , and  $\text{MgO}$  by repeated heating and grinding cycles (Turnock et al., 1973). Samples were suspended from Pt wire hangers and heated in air at temperatures 10–60 °C below the solidus in the range 1330–1350 °C at 1 atm pressure. Samples were quenched in 1 min to less than 300 °C by dropping the pellet from the furnace. After each experiment, the product was ground for 15 min under xylol in an alundum or agate mortar. After 2–3 cycles, the synthesis products contained mainly prismatic clinopyroxene crystals up to 30  $\mu\text{m}$  in length, with rare (~1%) olivine,  $\text{NiO}$  (~5% in nickel-diopside) and cristobalite (<5%). Synthesis conditions are listed in Table 1.

#### Data collection

Samples were mounted in standard Al sample holders with cavities of 20 × 15 × 1.6 mm. Thus with a 1° divergence slit, the irradiated area was confined to the sample at  $2\theta$  angles greater than 19°. Two mounting methods were used. For cell-dimension determination, powders were densely packed from the back of the mount against a frosted glass slide; this procedure gives a flat surface level with the top of the holder, a surface that is consis-

**TABLE 1.** Nominal compositions, conditions, and products

Experiment no.	Composition	T (°C)	Products
Ni <sub>100</sub>	CaNiSi <sub>2</sub> O <sub>6</sub>	1350	cpx + (NiO) + (crs)
Ni <sub>80</sub>	CaNi <sub>0.8</sub> Mg <sub>0.2</sub> Si <sub>2</sub> O <sub>6</sub>	1350	cpx + (NiO) + (crs)
Ni <sub>50</sub>	CaNi <sub>0.50</sub> Mg <sub>0.50</sub> Si <sub>2</sub> O <sub>6</sub>	1340	cpx + (NiO) + (crs)
Ni <sub>25</sub>	CaNi <sub>0.25</sub> Mg <sub>0.75</sub> Si <sub>2</sub> O <sub>6</sub>	1340	cpx + (NiO) + (crs)
Ni <sub>0</sub> *	CaMgSi <sub>2</sub> O <sub>6</sub>	1330	cpx + (crs)

Note: cpx: clinopyroxene; crs: cristobalite. Parentheses indicate amounts <5%.

\* Synthetic diopside (Raudsepp et al., 1990).

tent from sample to sample. In addition, specimen displacement and transparency errors are minimized (Wilson, 1963). Intensity data measured in this fashion are unsuitable for structure refinement because the tight packing against a flat surface greatly exaggerates preferred orientation. Mounts for intensity profile collection were made by loading the powder from the front of the holder. A straightedge was used to level the sample surface to that of the holder, and the surface was finely serrated several times with a razor blade; each pass with the razor blade was at right angles to the previous one. This technique tends to randomize the orientation of anisotropic crystals that are aligned during filling but maintains a generally flat surface.

Step-scan powder diffraction data<sup>1</sup> were obtained with a Philips automated diffractometer system PW1710, using a PW1050 Bragg-Brentano goniometer equipped with incident- and diffracted-beam Soller slits, 1° divergence and antiscatter slits, a 0.2-mm receiving slit, and a curved graphite diffracted-beam monochromator. The normal-focus Cu X-ray tube was operated at 40 kV and 40 mA,

<sup>1</sup> A copy of the observed and calculated step intensities may be ordered as Document AM-90-444 from the Business Office, Mineralogical Society of America, 1130 Seventeenth Street, Suite 330, Washington, DC 20036, U.S.A. Please remit \$5.00 in advance for the microfiche.

using a take-off angle of 6°. The profiles were obtained using a step interval of 0.12° 2θ, with a step counting time of 2 s. As discussed by Hill and Madsen (1986), these are approximately the optimum parameters for reducing serial correlation without adversely affecting the accuracy of these results. Information pertinent to data collection is given in Table 2.

**Rietveld structure refinement**

Structures were refined with the Rietveld program LHPM1 (DBW 3.2 originally written by Wiles and Young, 1981; modified by Hill and Howard, 1986). The peaks were defined as pseudo-Voigts with variable percentage Lorentzian character. The peak full-width at half-maximum (FWHM) was varied as a function of 2θ using the expression of Caglioti et al. (1958); peak asymmetry was corrected using the semiempirical relation of Rietveld (1969). The profile step intensity was calculated over the interval of four to six FWHM on either side of each peak centroid. Backgrounds were fitted with a simple polynomial function. Initial structural parameters were taken either from the single-crystal study of diopside (Levien and Prewitt, 1981), or from that of synthetic CaNiSi<sub>2</sub>O<sub>6</sub> (Ghose et al., 1987) depending on the Ni content. Isotropic displacement factors were fixed at the single-crystal values for CaNiSi<sub>2</sub>O<sub>6</sub>; for all Mg-bearing compositions, the diopside single-crystal values were used. Although preferred orientation was minor to nil in these samples, a correction for platey crystallites of the form  $I_{corr} = I_{calc} [P1 + (1 - P2)\exp(P1\alpha_k^2)]$  gave slightly lower agreement indices and more realistic structural parameters for some samples (P1 and P2 are refinable parameters, and α<sub>k</sub> is the acute angle between the scattering vector and the normal to the crystallites; P2 was not refined). Information pertinent to the structure refinements is given in Table 2.

After estimating as closely as possible the initial structural and experimental parameters both from the single-crystal structure and by inspection of the pattern, refinements were done in the following sequence. The scale

**TABLE 2.** Data measurement and details of structure refinement

	Ni <sub>100</sub>	Ni <sub>80</sub>	Ni <sub>50</sub>	Ni <sub>25</sub>	Ni <sub>0</sub> *
2θ scan range (°)	17–130	17–130	17–130	17–111	17–130
Step interval (°2θ)	0.12	0.12	0.12	0.12	0.12
Integration time/step (s)	2	2	2	2	2
Maximum step intensity (counts)	7333	6560	5536	6998	3185
No. of unique reflections	392	392	392	292	394
No. of structure parameters	19	20	20	20	19
No. of experimental parameters	13	12	13	13	13
N - P	911	910	910	751	911
R <sub>p</sub>	6.6	6.2	6.3	7.7	7.2
R <sub>wp</sub>	8.5	8.2	8.4	10.0	9.7
R <sub>z</sub>	3.7	2.7	2.7	3.5	3.3
Durbin-Watson d-statistic	1.80	1.66	1.92	1.86	1.39
U	0.011	0.033	0.072	0.029	0.049
V	0.002	-0.033	-0.027	-0.008	-0.020
W	0.026	0.042	0.037	0.020	0.104
γ <sub>1</sub>	0.422	0.277	0.400	0.555	0.355
γ <sub>2</sub>	0.003	0.004	0.002	0.009	0.006

Note: N - P = no. of observations (steps) - no. of least-squares parameters.

\* Synthetic diopside (Raudsepp et al., 1990).

TABLE 3. Cell dimensions of clinopyroxene

	<i>a</i> (Å)	<i>b</i> (Å)	<i>c</i> (Å)	$\beta$ (°)	<i>V</i> (Å <sup>3</sup> )
Ni-Di*	9.734(2)	8.891(2)	5.228(1)	105.87(2)	435.21(16)
Ni <sub>100</sub>	9.7359(4)	8.8932(4)	5.2284(3)	105.830(3)	435.52(4)
Ni <sub>80</sub>	9.7372(4)	8.8986(4)	5.2313(2)	105.826(4)	436.10(3)
Ni <sub>50</sub>	9.7390(5)	8.9094(4)	5.2375(2)	105.848(3)	437.18(3)
Ni <sub>25</sub>	9.7393(7)	8.9095(6)	5.2418(4)	105.850(8)	437.55(5)
Ni <sub>0</sub> **	9.7470(7)	8.9235(4)	5.2524(4)	105.939(4)	439.28(5)
Di†	9.7456(7)	8.9198(8)	5.2516(5)	105.86(1)	439.13(6)

\* CaNiSi<sub>2</sub>O<sub>6</sub> (Ghose et al., 1987).

\*\* Synthetic diopside (Raudsepp et al., 1990).

† Diopside (Levien and Prewitt, 1981).

factor, zero-point correction, background parameters, and cell dimensions were refined with all other parameters fixed. Next, the half-width parameters were refined; these are the most difficult parameters to refine, and occasionally some manual adjustment was necessary in order to achieve convergence. The remaining parameters were added to the refinement in the order: peak shape (percentage Lorentzian character), peak asymmetry, atomic positions, site occupancies, and correction for preferred orientation. Final convergence of the refinements was assumed when the parameter shifts in the final cycle were less than 30% of their respective standard deviations. Full details of the refinement technique are given by Raudsepp et al. (1990).

### EXPERIMENTAL RESULTS

Cell dimensions are given in Table 3, final atomic positions are given in Table 4, and the refined site occupancies are listed in Table 5. As shown in Table 2, the Durbin-Watson *d*-statistic (Durbin and Watson, 1950, 1951,

TABLE 5. Refined site occupancies for synthetic clinopyroxene

		Ni <sub>0</sub> *	Ni <sub>25</sub>	Ni <sub>50</sub>	Ni <sub>80</sub>	Ni <sub>100</sub>
M(1)	Mg	1.00	0.78(1)	0.55(1)	0.26(1)	0.00(1)
	Ni	—	0.22(1)	0.45(1)	0.74(1)	1.00(1)
M(2)	Ca	0.89(2)	1.00(1)	1.00(1)	1.00(1)	1.00(1)
	Mg	0.11(2)	0.00(1)	0.00(1)	0.00(1)	0.00(1)

\* Synthetic diopside (Raudsepp et al., 1990).

1971; Hill and Flack, 1987) is generally within the range  $2.0 \pm 0.2$ , indicative of insignificant serial correlation in the refinement process; this indicates that, except for the diopside composition, the assigned standard deviations should be accurate. Typical final observed, calculated, and difference X-ray powder diffraction patterns for the intermediate composition Ni<sub>50</sub> (CaMg<sub>0.55</sub>Ni<sub>0.45</sub>Si<sub>2</sub>O<sub>6</sub>) are shown in Figure 1.

### Site occupancies

A graphical comparison of the refined and nominal M(1) Ni contents is given in Figure 2; the refined occupancies are systematically less than the nominal Ni contents. There are two possible explanations for this: (1) the pyroxenes are off the nominal compositions; (2) the refinement results have a systematic error. Careful optical examination of the experimental products showed the presence of minor cristobalite and NiO. However, the amounts involved are not sufficient to account for the observed differences in Ni contents, and thus it must be concluded that our refinement results are not accurate.

It is notable that the refined M(1) Ni occupancies agree with the nominal compositions for the ordered end-

TABLE 4. Atomic positions for diopside and synthetic clinopyroxenes

		Di*	Ni <sub>0</sub> **	Ni <sub>25</sub>	Ni <sub>50</sub>	Ni <sub>80</sub>	Ni <sub>100</sub>	Ni-Di†
M(1)	<i>x</i>	0	0	0	0	0	0	0
	<i>y</i>	0.90814(5)	0.9071(8)	0.9072(7)	0.9079(6)	0.9095(7)	0.9087(5)	0.90911(6)
	<i>z</i>	0.25	0.25	0.25	0.25	0.25	0.25	0.25
	<i>B</i> (Å <sup>2</sup> )	0.37	0.37	0.37	0.37	0.37	0.37	0.34
M(2)	<i>x</i>	0	0	0	0	0	0	0
	<i>y</i>	0.30144(3)	0.2995(5)	0.3000(6)	0.2994(5)	0.2985(5)	0.2983(6)	0.29816(1)
	<i>z</i>	0.25	0.25	0.25	0.25	0.25	0.25	0.25
	<i>B</i> (Å <sup>2</sup> )	0.635	0.635	0.635	0.635	0.635	0.635	0.59
T	<i>x</i>	0.28627(3)	0.2857(5)	0.2876(5)	0.2865(4)	0.2867(4)	0.2866(5)	0.28733(8)
	<i>y</i>	0.09330(3)	0.0943(5)	0.0905(6)	0.0934(5)	0.0938(6)	0.0924(6)	0.09298(9)
	<i>z</i>	0.22936(5)	0.2312(8)	0.2299(10)	0.2283(8)	0.2389(8)	0.2252(9)	0.22752(14)
	<i>B</i> (Å <sup>2</sup> )	0.349	0.349	0.349	0.349	0.349	0.349	0.33
O(1)	<i>x</i>	0.11550(7)	0.1144(9)	0.1158(9)	0.1150(8)	0.1153(8)	0.1157(9)	0.1153(2)
	<i>y</i>	0.08728(7)	0.0900(11)	0.0861(11)	0.0874(11)	0.0860(11)	0.0849(13)	0.0861(2)
	<i>z</i>	0.1422(1)	0.1420(16)	0.1407(20)	0.1439(16)	0.1453(16)	0.1403(17)	0.1414(4)
	<i>B</i> (Å <sup>2</sup> )	0.51	0.51	0.51	0.51	0.51	0.51	0.50
O(2)	<i>x</i>	0.36136(7)	0.3619(10)	0.3633(10)	0.3610(8)	0.3590(9)	0.3578(10)	0.3603(2)
	<i>y</i>	0.25013(8)	0.2516(9)	0.2488(10)	0.2519(8)	0.2532(10)	0.2540(11)	0.2508(2)
	<i>z</i>	0.3183(1)	0.3176(17)	0.3218(20)	0.3190(17)	0.3202(17)	0.3230(19)	0.3188(4)
	<i>B</i> (Å <sup>2</sup> )	0.65	0.65	0.65	0.65	0.65	0.65	0.59
O(3)	<i>x</i>	0.35083(7)	0.3499(11)	0.3490(11)	0.3514(10)	0.3505(10)	0.3503(10)	0.3514(2)
	<i>y</i>	0.01759(8)	0.0185(9)	0.0180(10)	0.0178(9)	0.0184(9)	0.0203(10)	0.0191(2)
	<i>z</i>	0.9953(1)	0.9974(21)	0.9928(25)	0.9961(21)	0.9901(22)	0.9921(26)	0.9939(2)
	<i>B</i> (Å <sup>2</sup> )	0.56	0.56	0.56	0.56	0.56	0.56	0.51

\* Diopside, single-crystal structure (Levien and Prewitt, 1981).

\*\* Synthetic diopside (Raudsepp et al., 1990).

† CaNiSi<sub>2</sub>O<sub>6</sub>, single-crystal structure (Ghose et al., 1987).

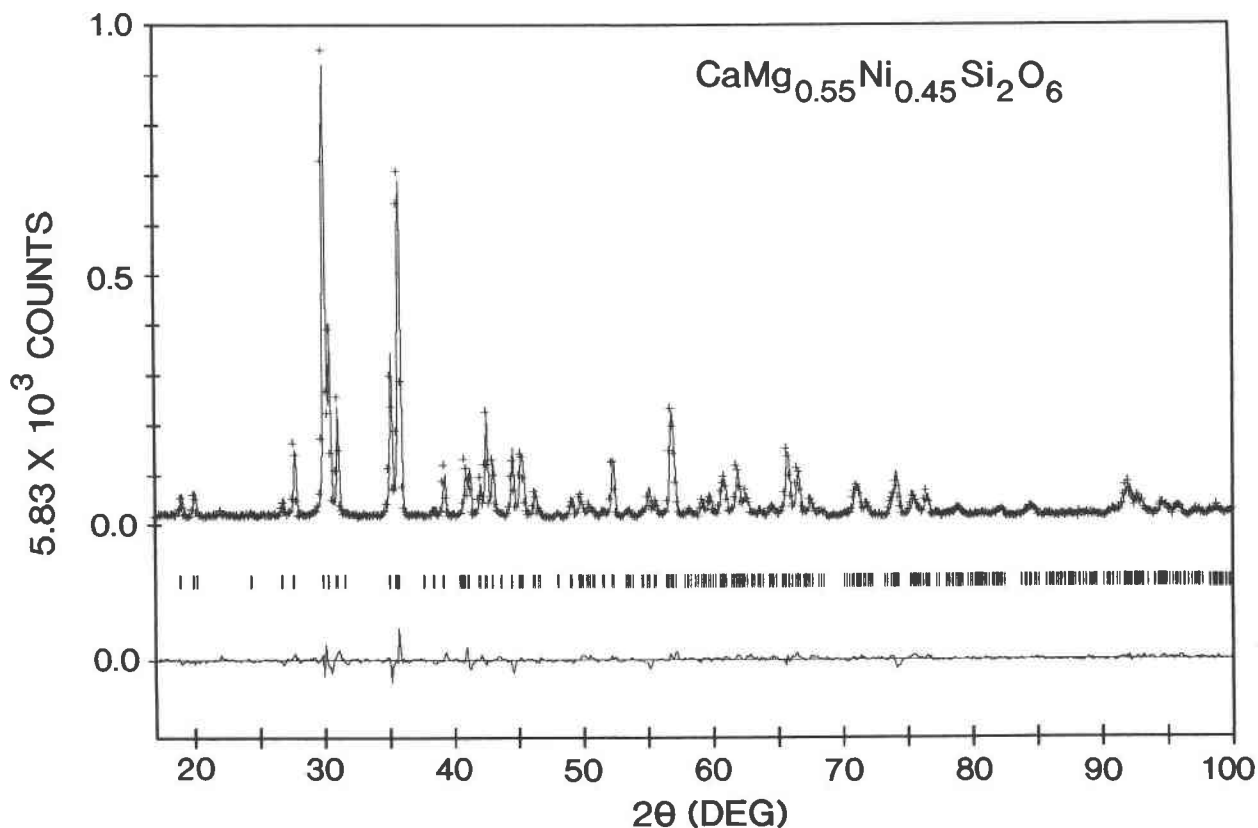


Fig. 1. Observed and calculated X-ray powder diffraction pattern for sample Ni<sub>50</sub> (CaMg<sub>0.55</sub>Ni<sub>0.45</sub>Si<sub>2</sub>O<sub>6</sub>). The crosses are the observed data, the solid line is the calculated pattern, and the vertical bars mark all possible Bragg reflections ( $K\alpha_1$  and  $K\alpha_2$ ). The difference between the observed and calculated patterns is shown at the bottom.

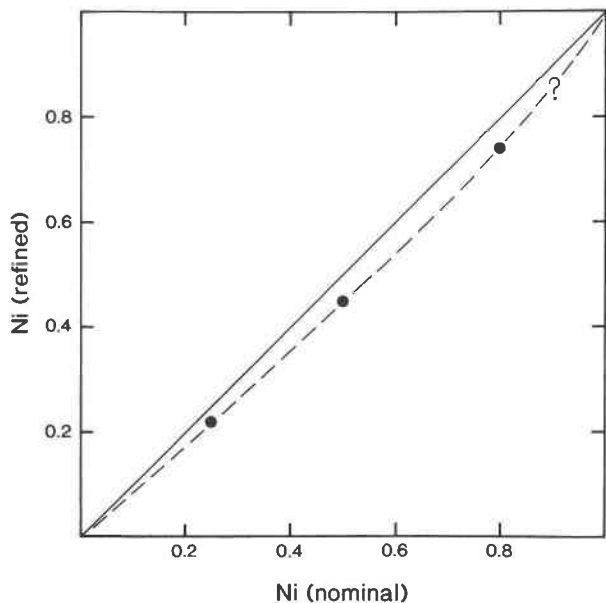


Fig. 2. Comparison of refined synthetic clinopyroxene M(1) site occupancies with nominal values for 100% synthesis of clinopyroxene.

member compositions and are too low for the intermediate solid solutions. There are two factors that are of significance here: (1) there is an inverse relationship between scattering power and displacement factor for an

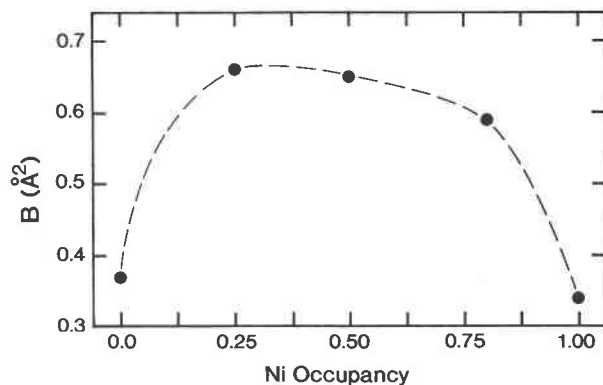


Fig. 3. Variation in M(1)-site isotropic displacement factors ( $B$ ) with Ni occupancy at the M(1) site. M(1) occupancies were fixed at nominal values; all other structural and pattern parameters [except M(1) displacement factors] were fixed at values from the final overall refinements.

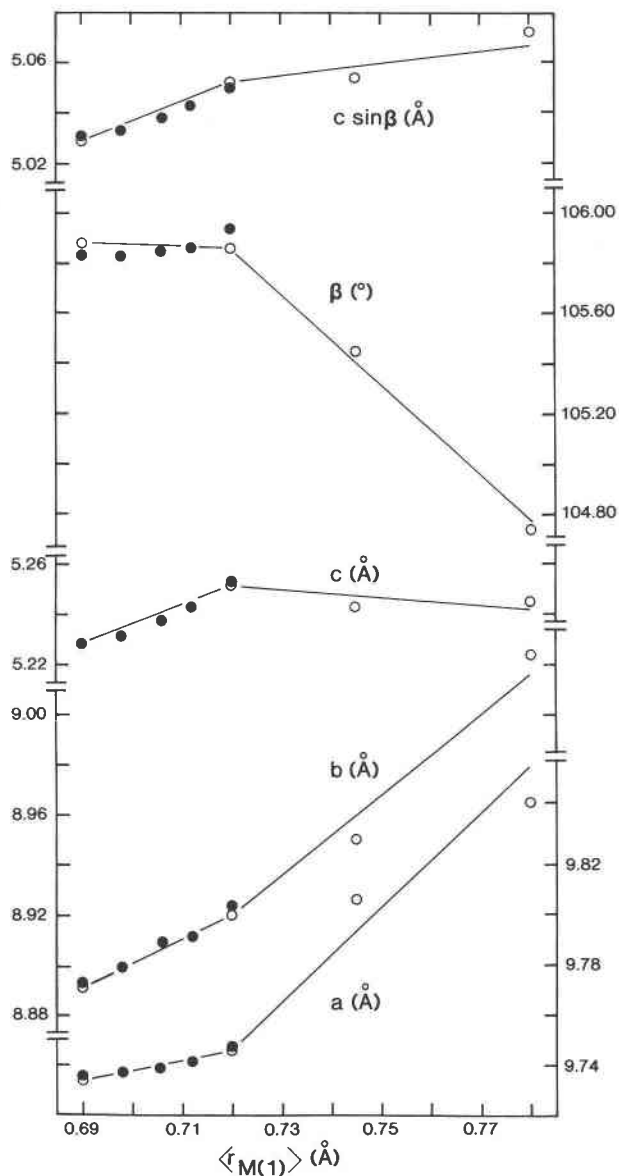


Fig. 4. Variation in cell parameters  $a$ ,  $b$ ,  $c$ ,  $\beta$  and  $c \sin \beta$  with mean ionic radius of the constituent cations at the M(1) site (solid circles). Open circles are data from the single-crystal structures of  $\text{CaNiSi}_2\text{O}_6$  and  $\text{CaCoSi}_2\text{O}_6$  (Ghose et al., 1987), diopside (Levien and Prewitt, 1981), and hedenbergite (Clark et al., 1969).

atom (site) in a crystal; (2) the displacement factors for sites involved in solid solutions are greater than the corresponding displacement factors in ordered end-members. In these refinements, the site occupancies and the displacement factors are not both refined, as the resolution of the data is normally not sufficient to allow such a procedure (at least in complex structures). Thus the refined site occupancies are sensitive to the displacement factors used. Taken together, the two points cited above suggest that too low a displacement factor has been used in the intermediate pyroxenes. Consequently larger values were

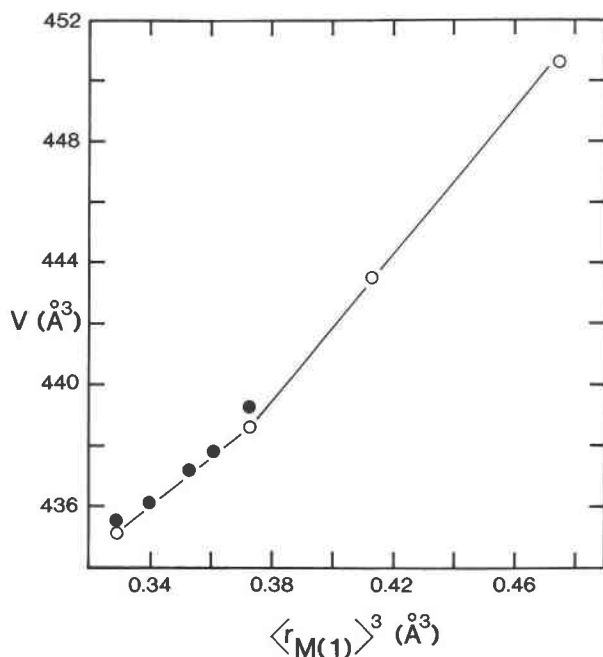


Fig. 5. Variation in cell volume with mean ionic radius cubed of the constituent cations at the M(1) site. Symbols are analogous to Figure 4.

experimented with in these intermediate refinements. As a final step, the occupancies were fixed at their nominal values and the corresponding displacement factors were refined; the results are shown in Figure 3. The displacement factors for the ordered end-members do not differ from the corresponding single-crystal values by more than two pooled standard deviations, whereas the displacement factors for the intermediate compositions refined to much larger values than the end-member displacement factors. This suggests that positional disorder may be contributing significantly to the displacement factors of the intermediate members; use of an inappropriately small displacement factor for sites of variable scattering power may result in refined occupancies that are systematically too low (in terms of the heavier scatterer). Although this does not significantly affect the arguments of the present work, it is obviously of importance to studies concerned with the accurate determination of site occupancies and bulk compositions; this point will be examined in detail in a subsequent study.

#### Cell dimensions

The variation in cell dimensions with constituent cation radii is shown in Figures 4 and 5; the range of calcic pyroxene compositions from Ni to Fe is shown to emphasize the anomalous nature of the diopside- $\text{CaNiSi}_2\text{O}_6$  series. In all cell parameters, there is a pronounced break in the linearity of the relationships at the diopside composition. Of course, this was well known from the previous single-crystal results on the ordered end-members. However, the results of the Rietveld refinements show

TABLE 6. Interatomic distances (Å) and angles (°) for diopside and synthetic clinopyroxenes

	Di*	Ni <sub>0</sub> **	Ni <sub>25</sub>	Ni <sub>50</sub>	Ni <sub>75</sub>	Ni <sub>100</sub>	Ni-Di†
T-O(1)	1.602(3)	1.606(8)	1.610(8)	1.608(7)	1.607(7)	1.602(8)	1.614(2)
T-O(2)	1.589(1)	1.594(8)	1.603(9)	1.599(8)	1.598(8)	1.616(9)	1.588(2)
T-O(3) <i>a</i>	1.669(3)	1.667(10)	1.652(12)	1.658(10)	1.679(10)	1.641(12)	1.663(2)
T-O(3) <i>b</i>	1.687(3)	1.697(10)	1.656(12)	1.692(10)	1.670(11)	1.692(12)	1.681(2)
⟨T-O⟩	1.637(1)	1.641(4)	1.630(5)	1.639(4)	1.638(5)	1.638(5)	1.637
⟨T-O⟩ <sub>nbr</sub>	1.596(2)	1.600(6)	1.607(6)	1.604(5)	1.603(5)	1.609(6)	1.601(1)
⟨T-O⟩ <sub>or</sub>	1.678(2)	1.682(7)	1.654(8)	1.675(7)	1.675(7)	1.667(8)	1.672(1)
M(1)-O(1) <i>c</i> × 2	2.119(2)	2.139(11)	2.120(11)	2.112(10)	2.089(10)	2.099(11)	2.101(2)
M(1)-O(1) <i>d</i> × 2	2.060(7)	2.055(8)	2.052(10)	2.061(8)	2.067(8)	2.045(8)	2.050(2)
M(1)-O(2) <i>e</i> × 2	2.051(2)	2.031(10)	2.045(10)	2.041(8)	2.056(9)	2.060(10)	2.059(2)
⟨M(1)-O⟩	2.076(2)	2.075(4)	2.072(4)	2.071(4)	2.070(4)	2.068(4)	2.070
M(2)-O(1) × 2	2.363(2)	2.325(10)	2.363(10)	2.339(9)	2.340(10)	2.356(11)	2.345(2)
M(2)-O(2) <i>f</i> × 2	2.346(8)	2.345(8)	2.317(10)	2.338(8)	2.338(8)	2.330(9)	2.336(2)
M(2)-O(3) <i>g</i> × 2	2.561(4)	2.580(9)	2.583(10)	2.568(9)	2.592(9)	2.602(10)	2.592(2)
M(2)-O(3) <i>h</i> × 2	2.721(4)	2.741(10)	2.727(12)	2.726(10)	2.710(11)	2.709(11)	2.711(2)
⟨M(2)-O⟩	2.498(3)	2.498(3)	2.497(3)	2.493(3)	2.495(3)	2.499(4)	2.496
Ti-O(3)-Tj	135.79(5)	136.1(6)	137.1(7)	135.6(6)	135.8(6)	135.7(6)	135.6(6)
O(3) <i>b</i> -O(3)-O(3) <i>j</i>	166.37(6)	165.7(7)	166.1(7)	166.2(7)	165.7(7)	164.3(7)	165.2(2)

Note: *a*: *x*, *y*, -1 + *z*; *b*: *x*, -*y*, -1/2 + *z*; *c*: *x*, 1 + *y*, *z*; *d*: *x*, 1 - *y*, 1/2 + *z*; *e*: 1/2 - *x*, 1/2 + *y*, 1/2 - *z*; *f*: 1/2 - *x*, 1/2 - *y*, 1 - *z*; *g*: 1/2 - *x*, 1/2 + *y*, 3/2 - *z*; *h*: 1/2 - *x*, 1/2 - *y*, 1 - *z*; *i*: *x*, *y*, 1 + *z*; *j*: *x*, -*y*, 1/2 + *z*.

\* Diopside, single-crystal structure (Levien and Prewitt, 1981).

\*\* Synthetic diopside, (Raudsepp et al., 1990).

† CaNiSi<sub>2</sub>O<sub>6</sub>, single-crystal structure (Ghose et al., 1987).

that this discontinuity occurs at the diopside composition rather than at some point along the diopside-CaNiSi<sub>2</sub>O<sub>6</sub> join. It is also apparent that these nonlinearities are significant: 0.04 Å for *a* and 0.025 Å for *b*. It is all the more surprising that the discrepancy in the *c* dimension is in the opposite direction: *c* is less than expected for a linear model (by 0.025 Å). It is obvious that the diopside-CaNiSi<sub>2</sub>O<sub>6</sub> solid solution responds very differently from the pyroxenes diopside-hedenbergite (and diopside-johannsenite, not shown) to variations in constituent M(1)-cation radii.

**Bond lengths**

The mean T-O bond lengths are constant across the series from Ni to Fe<sup>2+</sup> (Table 6). Conversely, ⟨M(1)-O⟩ decreases linearly from Fe<sup>2+</sup> to Mg (Fig. 6). At Mg, there is a very prominent break in slope, and ⟨M(1)-O⟩ then linearly decreases from M(1) = Mg to M(1) = Ni with a shallower slope. For the M(2) site, ⟨M(2)-O⟩ decreases across the series from Fe<sup>2+</sup> to Ni (Fig. 6). Although connecting the points shows a slight discontinuity at M(1) = Mg, this is not statistically significant in terms of either the Rietveld results or the more precise single-crystal results. Thus the principal discontinuity in these relationships is for the M(1) polyhedron, as might be expected.

A point to consider is whether or not the cation radius for Ni<sup>2+</sup> is the appropriate value. Shannon (1976) showed that chemical factors (such as the mean cation electronegativity) can affect mean bond lengths in crystals. For this reason, one does not look for exact agreement between observed mean bond lengths and constituent cation and anion radius sums; rather one looks for a linear variation in mean bond lengths with change in constituent cation (or anion) radius. This is not observed in the calcic pyroxenes, even though they are chemically very

similar materials. It is notable that the analogous olivine series M<sub>2</sub>SiO<sub>4</sub> (M = Ni, Mg, Co, Fe<sup>2+</sup>, Ca), shows well-developed linear relationships between mean bond lengths and constituent cation radii (Fig. 7). From this, it seems reasonable to conclude that the nonlinearity in the py-

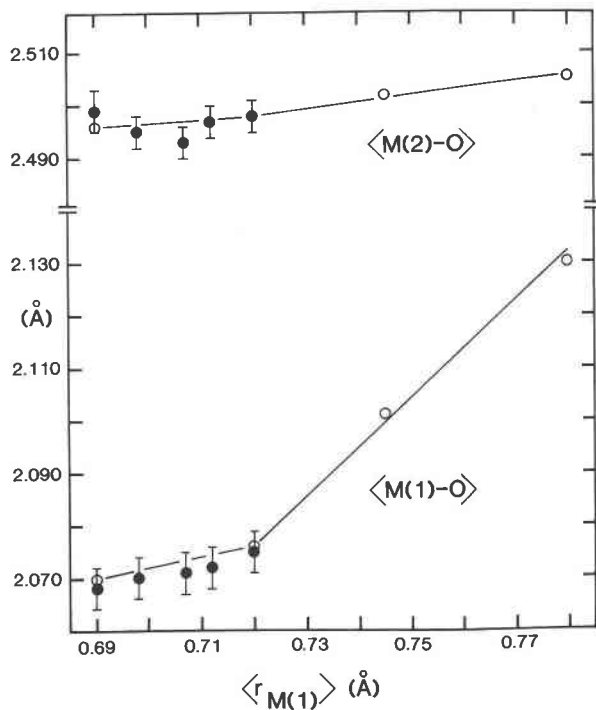


Fig. 6. Variation in ⟨M(1)-O⟩ and ⟨M(2)-O⟩ with mean ionic radius of the constituent cations at the M(1) site. Symbols are analogous to Figure 4.

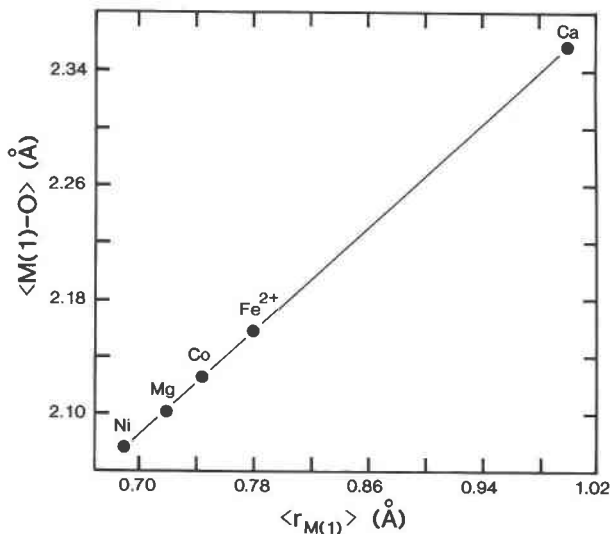


Fig. 7. Variation in  $\langle M(1)-O \rangle$  with constituent cation radius in synthetic ordered olivines.  $\text{Ni}_2\text{SiO}_4$ : Brown (1970);  $\text{Mg}_2\text{SiO}_4$ : Hazen (1976);  $\text{Co}_2\text{SiO}_4$ : Morimoto et al. (1974);  $\text{Fe}_2\text{SiO}_4$ : Hazen (1977);  $\text{Ca}_2\text{SiO}_4$ : Smith et al. (1965).

roxenes is a result of the pyroxene structure (i.e., its atomic arrangement) rather than the pyroxene chemistry.

Figure 8 shows the variation in  $\langle M(1)-O \rangle$  as a function of constituent cation radius for the pyroxene series  $\text{CaM}^{2+}\text{Si}_2\text{O}_6$  ( $M^{2+} = \text{Ni, Mg, Co, Fe, Mn}$ ),  $\text{NaM}^{3+}\text{Si}_2\text{O}_6$  ( $M^{3+} = \text{Al, Cr, Fe, Sc, In}$ ), and  $\text{CaM}^{3+}\text{SiM}^{3+}\text{O}_6$  ( $M^{3+} = \text{Al, Fe, Sc}$ ); note that each trend has been displaced vertically by 0.05 Å for clarity. None of these series shows perfect linearity; there are deviations at the high or at the low ends of the series. The most notable features of Figure 8 are as follows: (1) the linear trends in each series are parallel (slope = 0.89); (2) these linear trends correspond to the natural composition ranges of monoclinic pyroxenes; and (3) deviations at the upper ends of the series  $\text{NaM}^{3+}\text{Si}_2\text{O}_6$  and  $\text{CaM}^{3+}\text{SiM}^{3+}\text{O}_6$  are negative, such that the slope of the bond-length–cation-radius trend is decreased; deviations at the lower end of the series ( $\text{CaM}^{2+}\text{Si}_2\text{O}_6$ ) are positive, again such that the slope of the bond-length–cation-radius trend is decreased. The fact that the principal linear trends for each series are parallel and represent natural pyroxenes suggests that the pyroxene structure is most stable with this range of cation sizes for the relevant  $M(2)$ - and  $T$ -cation types. As the  $M(1)$ -cation size becomes less favorable, the structure no longer responds in the usual fashion, exhibiting anomalous trends as the limits of the structure stability are approached. It would be interesting to see if such behavior is related to the degree of ideality in the various solid-solution series for a particular structure type.

### CONCLUSIONS

There is complete solid solution along the diopside- $\text{CaNiSi}_2\text{O}_6$  join. The cell dimensions and some structural parameters are linear across the series but are not colinear

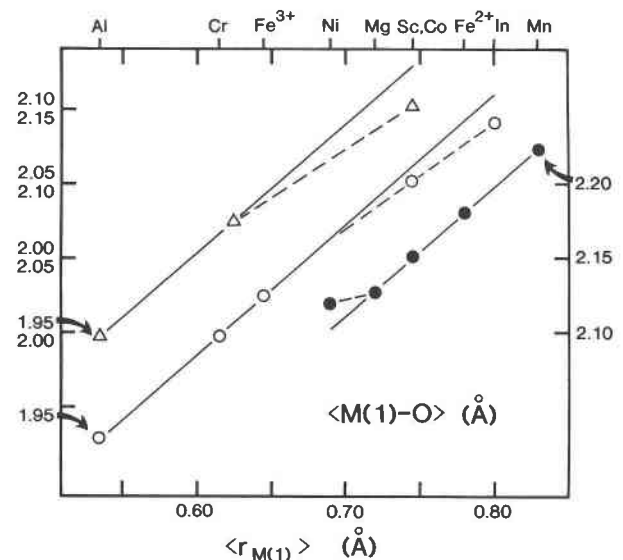


Fig. 8. Variation in  $\langle M(1)-O \rangle$  with constituent cation radius for the  $\text{CaM}^{2+}\text{Si}_2\text{O}_6$  (●),  $\text{NaM}^{3+}\text{Si}_2\text{O}_6$  (○), and  $\text{CaM}^{3+}\text{SiM}^{3+}\text{O}_6$  (△) pyroxene series; each series has been displaced 0.05 Å vertically for clarity. [References:  $\text{CaNiSi}_2\text{O}_6$ ,  $\text{CaCoSi}_2\text{O}_6$ : Ghose et al. (1987);  $\text{CaMgSi}_2\text{O}_6$ : Levien and Prewitt (1981);  $\text{CaFe}^{2+}\text{Si}_2\text{O}_6$ : Cameron et al. (1973);  $\text{CaMnSi}_2\text{O}_6$ : Freed and Peacor (1967);  $\text{NaAlSi}_2\text{O}_6$ ,  $\text{NaFe}^{3+}\text{Si}_2\text{O}_6$ ,  $\text{NaCrSi}_2\text{O}_6$ : Clark et al. (1969);  $\text{NaScSi}_2\text{O}_6$ : Hawthorne and Grundy (1973);  $\text{NaInSi}_2\text{O}_6$ : Hawthorne and Grundy (1974);  $\text{CaAlAlSiO}_6$ : Okamura et al. (1974);  $\text{CaFe}_{0.82}\text{Al}_{0.18}\text{Si}_{0.5}\text{Al}_{0.41}\text{Fe}_{0.09}\text{O}_6$ : Ghose et al. (1986);  $\text{CaScAlSiO}_6$ : Ohashi and Ii (1978)].

with the corresponding trends in the rest of the calcic pyroxenes. In particular, the trend of  $\langle M(1)-O \rangle$  vs.  $M(1)$ -cation radius deviates strongly from those of the other calcic pyroxenes and has a slope of only 0.20, compared with the general pyroxene slope of 0.89 and the hard-sphere model value of 1.0. We suggest that such anomalous relationships are characteristic of a structure type close to the limits of its stability with regard to cation size.

### ACKNOWLEDGMENTS

We thank D.L. Bish and an anonymous reviewer for their helpful comments. Financial assistance was provided by the Natural Sciences and Engineering Research Council of Canada in the form of operating grants to F.C. Hawthorne and A.C. Turnock and an infrastructure grant to F.C. Hawthorne.

### REFERENCES CITED

- Brown, G.E. (1970) The crystal chemistry of the olivines. Ph.D. thesis, Virginia Polytechnic Institute and State University, Blacksburg, Virginia.
- Caglioti, G., Paoletti, A., and Ricci, F.P. (1958) Choice of collimators for a crystal spectrometer for neutron diffraction. *Nuclear Instruments*, 3, 223–228.
- Cameron, M., and Papike, J.J. (1981) Structural and chemical variations in pyroxenes. *American Mineralogist*, 66, 1–50.
- Cameron, M., Sueno, S., Papike, J.J., and Prewitt, C.T. (1973) High-temperature crystal chemistry of acmite, diopside, hedenbergite, jadeite, spodumene, and ureyite. *American Mineralogist*, 58, 594–618.

- Clark, J.R., Appleman, D.E., and Papike, J.J. (1969) Crystal-chemical characterization of clinopyroxenes based on eight new structure refinements. *Mineralogical Society of America Special Paper*, 2, 31–50.
- Durbin, J., and Watson, G.S. (1950) Testing for serial correlation in least squares regression. I. *Biometrika* 37, 409–428.
- (1951) Testing for serial correlation in least squares regression. II. *Biometrika* 38, 159–178.
- (1971) Testing for serial correlation in least squares regression. III. *Biometrika* 58, 1–19.
- Freed, R.L., and Peacor, D.R. (1967) Refinement of the crystal structure of johannsenite. *American Mineralogist*, 52, 709–720.
- Ghose, S., Okamura, F.P., and Ohashi, H. (1986) The crystal structure of  $\text{CaFe}^{3+}\text{SiAlO}_6$  and crystal chemistry of  $\text{Fe}^{3+}$ - $\text{Al}^{3+}$  substitution in calcium Tschermak's pyroxene. *Contributions to Mineralogy and Petrology*, 92, 530–535.
- Ghose, S., Wan, Ch'eng, and Okamura, F.P. (1987) Crystal structures of  $\text{CaNiSi}_2\text{O}_6$  and  $\text{CaCoSi}_2\text{O}_6$  and some crystal-chemical relations in  $C2/c$  clinopyroxenes. *American Mineralogist*, 72, 375–381.
- Hawthorne, F.C., and Grundy, H.D. (1973) Refinement of the crystal structure of  $\text{NaScSi}_2\text{O}_6$ . *Acta Crystallographica*, B29, 2615–2616.
- Hawthorne, F.C., and Grundy, H.D. (1974) Refinement of the crystal structure of  $\text{NaInSi}_2\text{O}_6$ . *Acta Crystallographica*, B30, 1882–1884.
- Hazen, R.M. (1976) Effects of temperature and pressure on the crystal structure of forsterite. *American Mineralogist*, 61, 1280–1293.
- (1977) Effects of temperature and pressure on the crystal structure of ferromagnesian olivine. *American Mineralogist*, 62, 286–295.
- Hill, R.J., and Flack, H.D. (1987) The use of the Durbin-Watson d-statistic in Rietveld analysis. *Journal of Applied Crystallography*, 20, 356–361.
- Hill, R.J., and Howard, C.J. (1986) A computer program for Rietveld analysis of fixed-wavelength X-ray and neutron diffraction patterns. Report no. M112, Australian Atomic Energy Commission (now ANSTO), Lucas Heights Research Laboratories, Menai, New South Wales, Australia.
- Hill, R.J., and Madsen, I.C. (1986) The effect of profile step width on the determination of crystal structure parameters and estimated standard deviations by X-ray Rietveld analysis. *Journal of Applied Crystallography*, 19, 10–18.
- Levien, L., and Prewitt, C.T. (1981) High-pressure structural study of diopside. *American Mineralogist*, 66, 315–323.
- Morimoto, N., Tokonami, M., Watanabe, M., and Koto, K. (1974) Crystal structures of three polymorphs of  $\text{Co}_2\text{SiO}_4$ . *American Mineralogist*, 59, 475–485.
- Ohashi, H., and Ii, N. (1978) Structure of  $\text{CaScAlSiO}_6$ -pyroxene. *Journal of the Japanese Association for Mineralogy, Petrology and Economic Geology*, 73, 267–273.
- Okamura, F.P., Ghose, S., and Ohashi, H. (1974) Structure and crystal chemistry of calcium Tschermak's pyroxene,  $\text{CaAlAlSiO}_6$ . *American Mineralogist*, 59, 549–557.
- Post, J.E., and Bish, D.L. (1989) Rietveld refinement of crystal structures using powder X-ray diffraction data. *Reviews in Mineralogy*, 20, 277–308.
- Raudsepp, M., Hawthorne, F.C., and Turnock, A.C. (1990) Evaluation of the Rietveld method for the characterization of fine-grained products of mineral synthesis by Rietveld structure refinement: The diopside-hedenbergite join. *Canadian Mineralogist*, 28, 93–109.
- Ribbe, P.H., and Prunier, A.R., Jr. (1977) Stereochemical systematics of ordered  $C2/c$  pyroxenes. *American Mineralogist*, 62, 710–720.
- Rietveld, H.M. (1969) A profile refinement method for nuclear and magnetic structures. *Journal of Applied Crystallography*, 2, 65–71.
- Shannon, R.D. (1976) Systematic studies of interatomic distances in oxides. In R.G.J. Strens, Ed., *The physics and chemistry of minerals and rocks*, p. 403–431. Wiley, London.
- Smith, D.K., Majumdar, A., and Ordway, F. (1965) The crystal structure of  $\gamma$ -dicalcium silicate. *Acta Crystallographica*, 18, 787–795.
- Turnock, A.C., Lindsley, D.H., and Grover, J.E. (1973) Synthesis and unit cell parameters of Ca-Mg-Fe pyroxenes. *American Mineralogist*, 58, 50–59.
- Wiles, D.B., and Young, R.A. (1981) A new computer program for Rietveld analysis of X-ray powder diffraction patterns. *Journal of Applied Crystallography*, 14, 149–151.
- Wilson, A.J.C. (1963) *Mathematical theory of X-ray diffraction*. Centrex, Eindhoven, The Netherlands.
- Young, R.A. (1980) Structural analysis from X-ray powder diffraction patterns with the Rietveld method. Symposium on Accuracy in Powder Diffraction, National Bureau of Standards, Gaithersburg, Maryland, 143–163.

MANUSCRIPT RECEIVED FEBRUARY 10, 1990

MANUSCRIPT ACCEPTED OCTOBER 11, 1990